Article ID: 1000-324X(2020)04-0505-06 **DOI:** 10.15541/jim20190125

Synthesis, Crystal Structure, and Electrical Conductivity of Pd-intercalated $NbSe_2$

HUANG Chong[1,2], ZHAO Wei[1], WANG Dong[1], BU Kejun[1,2], WANG Sishun[1], HUANG Fuqiang[1,3]

(1. State Key Laboratory of High Performance Ceramics and Superfine Microstructure, Shanghai Institute of Ceramics, Chinese Academy of Sciences, Shanghai 200050, China; 2. University of Chinese Academy of Sciences, Beijing 100049, China; 3. State Key Laboratory of Rare Earth Materials Chemistry and Applications and Beijing National Laboratory for Molecular Sciences, College of Chemistry and Molecular Engineering, Peking University, Beijing 100871, China)

Abstract: New intercalated compounds Pd_xNbSe_2 (x=0-0.17) were synthesized *via* solid-state reaction. They possess the parent structure of 2H-$NbSe_2$ and crystalize in the hexagonal space group of $P6_3/mmc$. The intercalated Pd occupies the octahedral position in the van der Waals gaps of 2H-$NbSe_2$. Unit cell parameter c increases linearly with the Pd content, while a is nearly unchanged. The lattice parameter of $Pd_{0.17}NbSe_2$ (a=b=0.34611(2) nm, c=1.27004(11) nm) is identified by single crystal X-ray diffraction. The intercalated Pd stabilizes the crystal structure of $NbSe_2$ by connecting the adjacent Nb-Se layers with [$PdSe_6$] octahedra and leads to the enhanced thermostability in air. Temperature dependence of electric resistivity reveals that the residual resistivity ratio of Pd_xNbSe_2 monotonically decreases with addition of the intercalated Pd content. The decreased superconducting critical temperature of Pd_xNbSe_2 indicates the suppression effect of Pd intercalation on the superconductivity in the host $NbSe_2$.

Key words: Pd_xNbSe_2; transition metal dichalcogenide; crystal structure; superconducting

Layered transition metal dichalcogenides (TMDs) with the general chemical formula MX_2 (M represents the transition metal and X is the chalcogen) have been widely studied due to their unique physicochemical properties and diverse applications[1-5]. The metallic Group Ⅴ B TMDs (where M = V, Nb and Ta) are prized for their fascinating electronic properties, such as charge density wave (CDW), superconductivity and Mott transition[6-7]. Among them, 2H-$NbSe_2$ is featured with a high superconducting critical temperature (T_C) of ~7.3 K and a quasi-two-dimensional incommensurate charge density wave (ICDW) with a T_{CDW} of ~33 K[8]. Because of the weak van der Waals (vdW) forces connected interlayers in the crystal structure, 2H-$NbSe_2$ can be intercalated by various guests, including atoms, ions, and molecules[9].

Typically, the incorporation of guest metal atoms into the vdW gaps of TMDs could give rise to the crystallographic transformation and change of electronic structure in the intercalated compounds[10]. Magnetic elements (Fe, Co) inserted into the vdW gaps of $NbSe_2$ resulted in the formation of superlattice[11-12]. Alkali metal intercalation was found to remove the CDW instability in $NbSe_2$[13]. Recently, noble metal, such as palladium (Pd), was applied to regulate the electronic structure efficiently for the host TMDs. Our group[14] found that Pd modified the band structure of 2H-TaS_2 through Pd−S bonding to strengthen the interaction of adjacent Ta-S layers, which led to the enhanced conductivity in $Pd_{0.10}TaS_2$. Pd intercalation was reported to increase the effective electron-phonon coupling in 2H-$TaSe_2$ and enhance the T_C in Pd_xTaSe_2[15]. Considering that the crystal structure of 2H-$NbSe_2$ is identical to that of 2H-TaX_2 (X=S, Se), Pd intercalation should be applicable to 2H-$NbSe_2$ and tune the physical properties.

In this work, a series of new compounds Pd_xNbSe_2 (x=0~0.17) were synthesized and the crystal structure of $Pd_{0.17}NbSe_2$ was determined by single X-ray diffraction method in order to investigate the modification of crystal lattice and electrical conductivity in the Pd intercalated $NbSe_2$.

Received date: 2019-03-26; **Revised date:** 2019-04-30

Foundation item: National Key Research and Development Program (2016YFB0901600); Science and Technology Commission of Shanghai (16JC1401700, 16ZR1440500); National Natural Science Foundation of China (Y93GJ11101); The Key Research Program of Chinese Academy of Sciences (QYZDJ-SSW-JSC013, KGZD-EW-T06); CAS Center for Excellence in Superconducting Electronics, and Youth Innovation Promotion Association CAS

Biography: HUANG Chong (1994–), male, Master candidate. E-mail: huangchong@student.sic.ac.cn
黄 冲(1994–), 男, 硕士研究生. E-mail: huangchong@student.sic.ac.cn

Corresponding author: HUANG Fuqiang, professor. E-mail: huangfq@mail.sic.ac.cn; ZHAO Wei, associate professor. E-mail: zhaowei220@mail.sic.ac.cn
黄富强, 研究员. E-mail: huangfq@mail.sic.ac.cn; 赵 伟, 副研究员. E-mail: zhaowei220@mail.sic.ac.cn

1 Experimental

1.1 Preparation of Pd_xNbSe_2

Pd_xNbSe_2 crystals were prepared by solid-state reaction. Pd (99.99%), Nb (99.5%) and Se (99.99%) powders were mixed according to stoichiometric ratio, and ground. Then the mixtures were compacted into a pellet and heated in the evacuated (< 0.133 Pa) silica tube at 1173 K for 48 h. Subsequently, the as-obtained samples were reground, re-pelletized and held at 1173 K for 72 h. Then the samples were cooled down by quenching in water. High quality single crystal of $Pd_{0.17}NbSe_2$ was obtained by keeping $Pd_{0.17}NbSe_2$ powder with CsI (99.9%) at 1173 K for 1 d and slowly cooling down to 823 K for 3 d.

1.2 Characterization

Single crystal data collections of $Pd_{0.17}NbSe_2$ was conducted on a Bruker D8 QUEST diffractometer equipped with Mo Kα radiation at room temperature. The crystal structure determination and refinement were performed with the APEX3 program. The crystal structure of $Pd_{0.17}NbSe_2$ was drawn by using the VESTA program[16]. The morphology and the composition of the $Pd_{0.17}NbSe_2$ were investigated by a scanning electron microscope (SEM, JSM6510) coupled with energy dispersive X-ray spectroscopy (EDXS, Oxford Instruments). The micro-structure of $Pd_{0.17}NbSe_2$ was uncovered by a high-resolution transmission electron microscope (HRTEM, JEM-2100F) and the selected area electron diffraction (SAED). The valence analysis of the $Pd_{0.17}NbSe_2$ was obtained from X-ray photoelectron spectroscope (XPS) carried out on the RBD upgraded PHI-5000C ESCA system (PerkinElmer) with Mg Kα radiation ($h\nu$=51253.6 eV). The binding energy in XPS analysis was corrected by referencing C 1s peak at 284.6 eV. Powder X-ray diffraction (PXRD) data of these Pd_xNbSe_2 samples were collected by using a Bruker D8QUEST diffractometer equipped with Cu Kα radiation (λ=0.15405 nm). Thermogravimetric analysis (TG) and differential thermal analysis (DTA) were carried out on a NETZSCH STA449C thermal analyzer for investigating the thermal stability of $Pd_{0.17}NbSe_2$ and $NbSe_2$ in air. Resistivity of the as-obtained Pd_xNbSe_2 at different temperatures was executed on a Physical Properties Measurement System (PPMS, Quantum Design). A four-probe method was adopted for measurements of the resistance. More specifically, the powders were pressed into a disk. Silver paste and copper wire acted as the contact electrode and conduct wire, respectively. Normalized resistivity ($\rho/\rho_{300\,K}$) *versus* temperature curves were obtained via dividing the measured resistivity (ρ) by the resistivity value ($\rho_{300\,K}$) at room temperature.

2 Results and discussion

The crystal structure of $Pd_{0.17}NbSe_2$ identified by single crystal X-ray diffraction method is shown in Fig. 1(a-b), where the gray, blue, orange spheres represent Pd, Nb, and Se atoms, respectively. The crystal data and structure refinement of $Pd_{0.17}NbSe_2$ are given in Table 1. The fractional atomic coordinates and equivalent isotropic displacement parameters are summarized in Table S1. The atomic displacement parameters and the geometric pa rameters

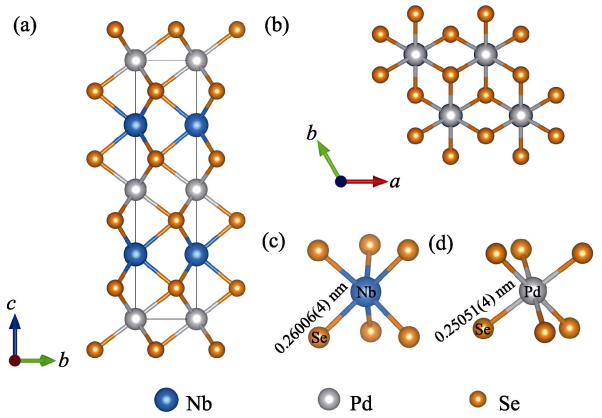

Fig. 1 Crystal structure of $Pd_{0.17}NbSe_2$ along (a) the *bc*-plane and (b) the *ab*-plane, (c) [$NbSe_6$] triangular prism in $Pd_{0.17}NbSe_2$, (d) [$PdSe_6$] octahedron in $Pd_{0.17}NbSe_2$

Table 1 Crystal data and structure refinement of $Pd_{0.17}NbSe_2$

Chemical formula	$Pd_{0.17}NbSe_2$
M_r/(g·mol^{-1})	269.03
Crystal system	Hexagonal, $P6_3/mmc$
a, c/nm	0.34611(2), 1.27004(11)
V/nm^3	0.13176(2)
Z	2
Radiation type	Mo Kα, λ=0.071073 nm
Crystal color	Black
ρ_c/(g·cm^{-3})	6.781
μ/mm^{-1}	32.93
Crystal size/mm^3	0.01×0.01×0.003
Diffractometer	Bruker D8 QUEST
T_{min}, T_{max}	0.494, 0.746
No. of measured, independent and observed [$I > 2\sigma(I)$] reflections	1480, 121, 103
R_{int}	0.053
$(\sin\theta/\lambda)_{max}$/nm^{-1}	7.55
R_1, wR_2, S^a	0.019, 0.035, 1.14
No. of reflections	121
No. of parameters	9

$^aR_1=\Sigma||F_o|-|F_c||/\Sigma|F_o|$, $wR_2=[\Sigma w(F_o^2-F_c^2)^2/\Sigma(wF_o^2)^2]^{1/2}$, $w=1/[\sigma^2(F_o^2)+(aP)^2+bP]$, where F_o is the observed structure factor, F_c is the calculated structure factor, σ is the standard deviation of F_c^2, and $P=(F_o^2+2F_c^2)/3$. $S=[\Sigma w(F_o^2-F_c^2)^2/(n-p)]^{1/2}$, where n is the number of reflections and p is the total number of parameters refined.

are shown in Table S2–S3. The space group of $Pd_{0.17}NbSe_2$ is determined to be $P6_3/mmc$ with lattice parameters of a=0.34611(2) nm, c=1.27004(11) nm. $Pd_{0.17}NbSe_2$ contains one independent Nb site (2*b*), one independent Se site (4*f*) and one independent Pd site (2*a*). $Pd_{0.17}NbSe_2$ consists of Nb-Se layer and Pd-Se layer, which are stacked alternately along *c* axis. Each Nb atom is coordinated by 6 Se atoms which formed a [$NbSe_6$] triangular prism (Fig. 1(c)). The length of Nb−Se bond in [$NbSe_6$] triangular prism is 0.26006(4) nm which is comparable to 0.25941(5) nm in $NbSe_2$[17]. These [$NbSe_6$] triangular prisms are connected by edge-sharing to form the Nb-Se layer.

Each Pd atom is coordinated by 6 Se atoms to form [$PdSe_6$] octahedron (Fig. 1(d)). The average length of Pd−Se bond in [$PdSe_6$] octahedron is 0.25051(4) nm which is comparable to 0.248602(0) nm of $PdSe_2$[18]. These [$PdSe_6$] octahedra partially fill in the vdW gaps of $NbSe_2$, where the occupation of Pd sites is 17%.

The $Pd_{0.17}NbSe_2$ plate with the size about 5 μm was observed by SEM (Fig. 2(a)). The Pd atoms are in a homogenous dispersion in $Pd_{0.17}NbSe_2$, which is confirmed by the elemental mapping analysis of $Pd_{0.17}NbSe_2$. HRTEM image of $Pd_{0.17}NbSe_2$ (Fig. 2(b)) reveals that the lattice fringes with a spacing of 0.301 nm are assigned to (101) plane and $(1\bar{1}1)$ plane between which the angle is 60°. This result is also verified by the corresponding SAED.

XPS data was obtained to confirm the valence state variation of the elements in $Pd_{0.17}NbSe_2$. As displayed in Fig. 3(a), the Pd 3d region is the only difference between $Pd_{0.17}NbSe_2$ and $NbSe_2$. The Pd 3d region of

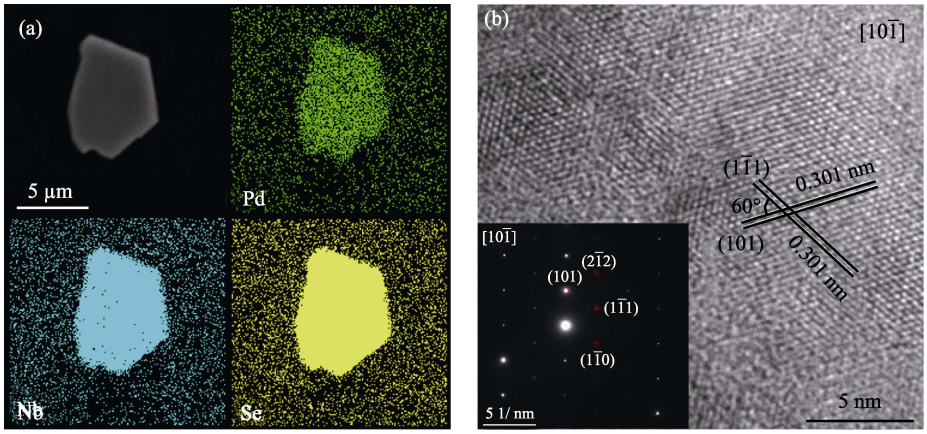

Fig. 2　(a) SEM images of $Pd_{0.17}NbSe_2$ and the corresponding elemental mapping analysis, and (b) HRTEM image of $Pd_{0.17}NbSe_2$ along [10$\bar{1}$] zone axis with inset showing the corresponding SAED pattern

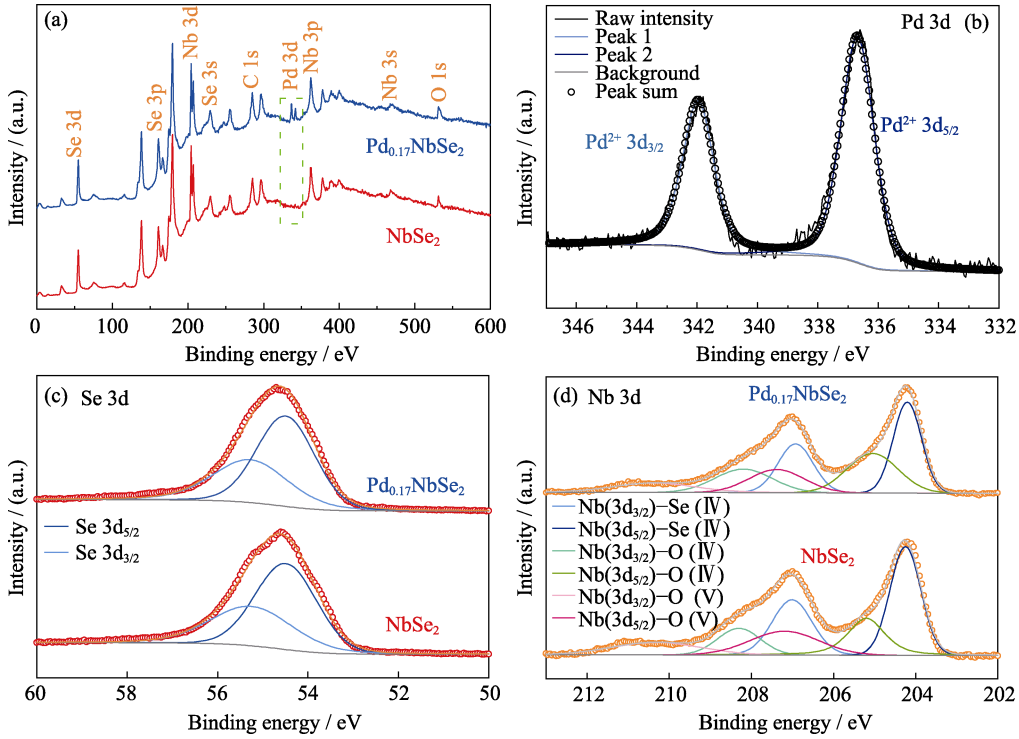

Fig. 3　XPS results of $Pd_{0.17}NbSe_2$ and $NbSe_2$
(a) Survey spectra, (b) Pd 3d spectrum of $Pd_{0.17}NbSe_2$, (c) Se 3d spectrum, and (d) Nb 3d spectrum

$Pd_{0.17}NbSe_2$ shows two peaks, which locate at the binding energy of 341.95 eV ($3d_{3/2}$) and 336.70 eV ($3d_{5/2}$) (Fig. 3(b)). The valance state of Pd in $Pd_{0.17}NbSe_2$ is identified as +2 according to these two peaks[14]. There are two peaks locating at 55.27 (Se $3d_{3/2}$) and 54.50 eV (Se $3d_{5/2}$) in the Se 3d region of $Pd_{0.17}NbSe_2$, similar to those in the Se 3d region of $NbSe_2$ (Se $3d_{3/2}$ at 55.25 eV and Se $3d_{5/2}$ at 54.49 eV) (Fig. 3(c)). Therefore, the valance state of Se in $Pd_{0.17}NbSe_2$ is considered as –2. The Nb 3d region shows a mixture of oxidation states because of the slightly oxidation of the samples (Fig. 3(d))[19]. The peaks locating at 206.93 and 204.20 eV are attributed to the Nb−Se bonding in $Pd_{0.17}NbSe_2$. In comparison with these two peaks in pristine $NbSe_2$ (207.01 and 204.25 eV), there is a slight redshift in $Pd_{0.17}NbSe_2$, implying the partial reduction of Nb as a result of Pd intercalation[14].

The intercalated amounts of Pd in $NbSe_2$ could be variable, resulting in the formation of a series of Pd_xNbSe_2. The powder XRD patterns of Pd_xNbSe_2 are displayed in Fig. 4(a), with the pristine $NbSe_2$ as reference. The peaks of $Pd_{0.17}NbSe_2$ are well matched to the simulated one obtained from single crystal data, which suggests a high degree of phase purity. The $NbSe_2$ still maintains its space group ($P6_3/mmc$) after Pd intercalation. The (004) peak gradually shifts to a lower angle compared with 2H-$NbSe_2$. Furthermore, the lattice parameter *a* undergoes a negligible change. In a sharp contrast, lattice parameter *c* increases remarkably because of Pd intercalation enlarging the interlayer space of $NbSe_2$ (Fig. 4(b)).

The influence of Pd intercalation on the thermostability of the samples was investigated. As clearly seen in Fig. 5(a), the weight of $NbSe_2$ begins to increase slightly at 559 K due to the formation of $Nb_2Se_4O_{13}$[20]. Subsequently, TG curve of $NbSe_2$ suffers a dramatic decrease because of the complete oxidation of $NbSe_2$ to Nb_2O_5. However, the process of mass increase could not be found in $Pd_{0.17}NbSe_2$, suggesting that the intercalated Pd enhances the thermostability of $NbSe_2$ with a higher oxidizing temperature. According to DTA curves (Fig. 5(b)), the oxidizing temperature of $Pd_{0.17}NbSe_2$ is 608 K, higher than $NbSe_2$ (544 K). The enhanced thermostability in air could stem from the intercalated Pd which stabilizes the crystal structure of $NbSe_2$ by connecting the adjacent Nb-Se layers[11,21-22].

The electrical conductivity of Pd_xNbSe_2 was measured by PPMS. The resistivity of Pd_xNbSe_2 increases with the rising temperature (Fig. S1) exhibiting metallic behavior. Moreover, the residual resistivity ratio (*RRR*) [(resistivity at 300 K)/(resistivity just above T_C)] for the $Pd_{0.17}NbSe_2$ is ~1.09, extremely lower than $NbSe_2$ (~7.67) (Fig. 6(a)).

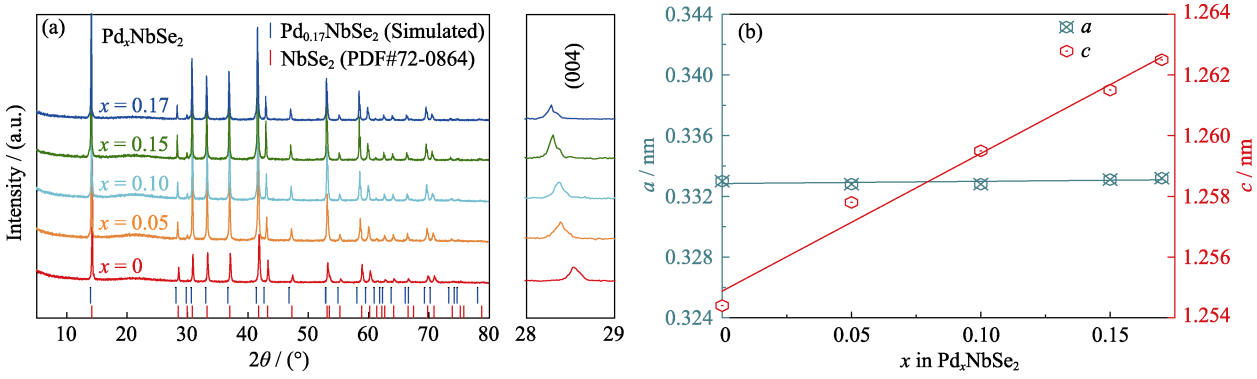

Fig. 4 (a) Powder XRD patterns of Pd_xNbSe_2 (x=0, 0.05, 0.10, 0.15, 0.17), (b) composition dependence of the lattice parameters *a* and *c* for Pd_xNbSe_2 ($0 \leqslant x \leqslant 0.17$)

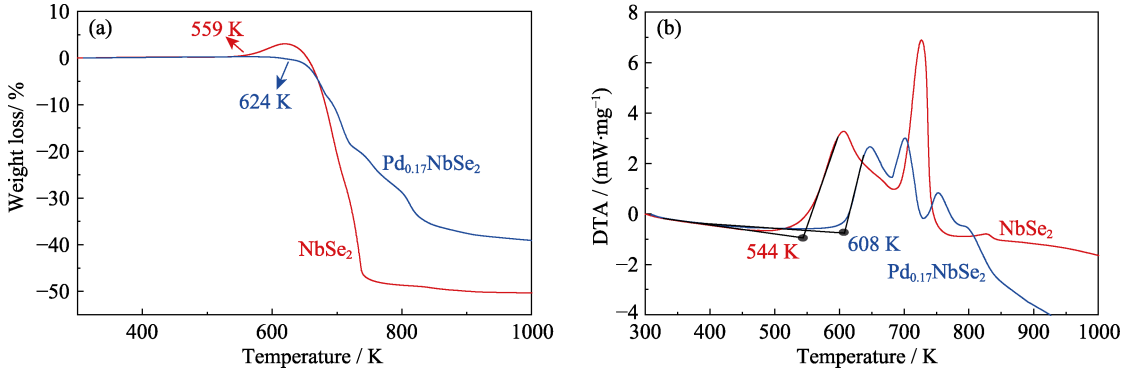

Fig. 5 (a) TG and (b) DTA curves of $Pd_{0.17}NbSe_2$ (blue) and $NbSe_2$ (red)

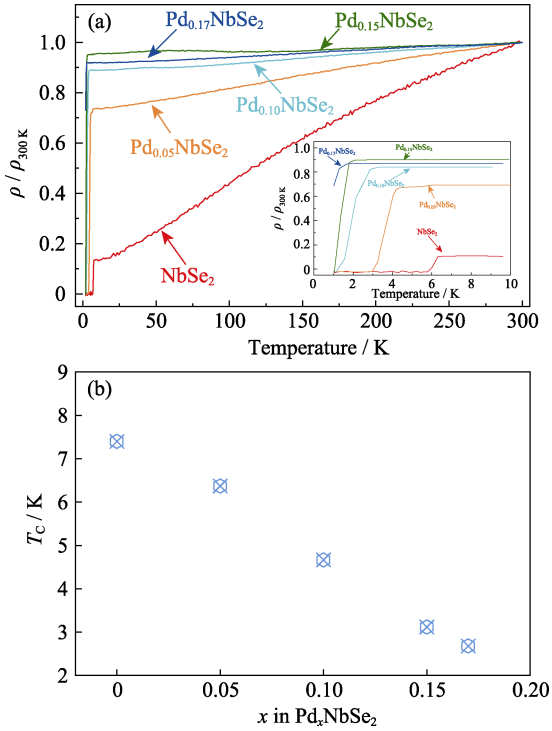

Fig. 6　(a) Temperature dependence of the RRR ($\rho/\rho_{300\ K}$) for Pd_xNbSe_2 ($0 \leqslant x \leqslant 0.17$) with inset showing enlarged temperature regionof the superconducting transition, (b) composition dependence of T_C

The poor *RRR* in $Pd_{0.17}NbSe_2$ indicates that the intercalated Pd may be an electronically disruptive dopant in $NbSe_2$, which is similar to the copper (Cu) in Cu_xNbSe_2 and the gallium (Ga) in Ga_xNbSe_2[8,23]. All of the Pd_xNbSe_2 samples exhibit a sharp decrease at low temperature region from 8 K to 2K, indicating that the superconductivity occurs in these samples. Fig. 6(b) shows that the T_C decreases with a higher intercalated amount of Pd (7.4 K for $NbSe_2$ and 2.7 K for $Pd_{0.17}NbSe_2$). Eventually, the zero resistivity cannot be observed at 2 K in $Pd_{0.17}NbSe_2$. Therefore, it declares that the intercalated Pd has a negative effect on the superconductivity in $NbSe_2$. Similar phenomena are also found in Cu_xNbSe_2, Ga_xNbSe_2, Fe_xNbSe_2 and Al_xNbSe_2[8,23-24]. The reason for this might be that Pd intercalation disrupts the coherence of the CDW, and suppresses the pairing channel which contributes to the higher T_C in $NbSe_2$[8].

3　Conclusions

In summary, we introduced noble metal Pd into the vdW gaps of $NbSe_2$, and synthesized a series of new intercalated compounds Pd_xNbSe_2. The $Pd_{0.17}NbSe_2$ crystalizes in hexagonal structure with cell parameter a= 0.34611(2) nm, c=1.27004(11) nm. The intercalated Pd stabilizes the crystal structure of $NbSe_2$ by connecting the adjacent Nb-Se layers with [$PdSe_6$] octahedra leading to the enhanced thermostability in air. Pd_xNbSe_2 remains the metallic character, which is verified by the resistivity measurements. In addition, the incorporation of Pd decreases the T_C of $NbSe_2$, implying that Pd is negative for the superconductivity in $NbSe_2$.

References:

[1] TAN CHAO-LIANG, CAO XIE-HONG, WU XUE-JUN, *et al*. Recent advances in ultrathin two-dimensional nanomaterials. *Chemical Reviews*, 2017, **117(9):** 6225–6331.

[2] GOPALAKRISHNAN D, LEE A, THANGAVEL N K, *et al*. Facile synthesis of electrocatalytically active NbS_2 nanoflakes for an enhanced hydrogen evolution reaction. *Sustainable Energy & Fuels*, 2018, **2(1):** 96–102.

[3] JIN HUAN-YU, GUO CHUN-XIAN, LIU XIN, *et al*. Emerging two-dimensional nanomaterials for electrocatalysis. *Chemical Reviews*, 2018, **118(13):** 6337–6408.

[4] WANG REN-YAN, GAN LIN, ZHAI TIAN-YOU. ReX_2 (X=S, Se): a new opportunity for development of two-dimensional anisotropic materials. *Journal of Inorganic Materials*, 2019, **34(1):** 1–16.

[5] ZHAO DE-RUI, ZHAI YING-JIAO, LI JIN-HUA, *et al*. Preparation and properties of glucose biosensor based on flower-like MoS_2 micrometer material. *Journal of Inorganic Materials*, 2016, **31(2):** 153–158.

[6] CHIA X, AMBROSI A, LAZAR P, *et al*. Electrocatalysis of layered group 5 metallic transition metal dichalcogenides (MX_2, M=V, Nb, and Ta; X = S, Se, and Te). *Journal of Materials Chemistry A*, 2016, **4(37):** 14241–14253.

[7] SIPOS B, KUSMARTSEVA A F, AKRAP A, *et al*. From Mott state to superconductivity in 1T-TaS_2. *Nature Materials*, 2008, **7(12):** 960–965.

[8] LUO HUI-XIA, STRYCHALSKA-NOWAK J, LI JUN, *et al*. S-shaped suppression of the superconducting transition temperature in Cu-intercalated $NbSe_2$. *Chemistry of Materials*, 2017, **29(8):** 3704–3712.

[9] WANG MENG-JING, WILLIAMS D, LAHTI G, *et al*. Chemical intercalation of heavy metal, semimetal, and semiconductor atoms into 2D layered chalcogenides. *2D Materials*, 2018, **5(4):** 045005.

[10] HAO QIAO-YAN, WANG DA-KE, ZHU BAI-CHUAN, *et al*. Facile synthesis, structure and physical properties of 3R-A_xNbS_2 (A=Li, Na). *Journal of Alloys and Compounds*, 2016, **663:** 225–229.

[11] PRODAN A, MARINKOVIC V, ROJSEK M, *et al*. The surface superstructures in niobium disulfide and diselenide intercalated by Cu, Co and Fe. *Surface Science*, 2001, **476(1):** 71–77.

[12] HUGHES T A, KEVAN S D, COX D E, *et al*. Synthesis of superlattices of intercalated transition metal dichalcogenides. *Journal of the American Chemical Society*, 2000, **122(37):** 8910–8915.

[13] LIAN CHAO-SHENG, SI CHEN, WU JIAN, *et al*. First-principles study of Na-intercalated bilayer $NbSe_2$: suppressed charge-density wave and strain-enhanced superconductivity. *Physical Review B*, 2017, **96(23):** 235426.

[14] WANG DONG, WANG XIN, LU YUE, *et al*. Atom-scale dispersed palladium in a conductive $Pd_{0.1}TaS_2$ lattice with a unique electronic structure for efficient hydrogen evolution. *Journal of Materials Chemistry A*, 2017, **5(43):** 22618–22624.

[15] BHOI D, KHIM S, NAM W, *et al*. Interplay of charge density wave and multiband superconductivity in 2H-Pd_xTaSe_2. *Scientific Reports*, 2016, **6:** 24068.

[16] MOMMA K, IZUMI F. VESTA 3 for three-dimensional visualization of crystal, volumetric and morphology data. *Journal of Applied Crystallography*, 2011, **44(6):** 1272–1276.
[17] MAREZIO M, DERNIER P, MENTH A, *et al*. The crystal structure of $NbSe_2$ at 15 K. *Journal of Solid State Chemistry*, 1972, **4(3):** 425–429.
[18] HAMIDANI A, BENNECER B, ZANAT K. Structural and electronic properties of the pseudo-binary compounds PdX_2 (X=P, S and Se). *Journal of Physics and Chemistry of Solids*, 2010, **71(1):** 42–46.
[19] ZHAO BEN-LIANG, HUANG JIAN, FU QI, *et al*. MoS_2/$NbSe_2$ hybrid nanobelts for enhanced hydrogen evolution. *Journal of The Electrochemical Society*, 2016, **163(6):** H384–H387.
[20] HALASYAMANI P S, O'HARE D. Synthesis and characterization of $Se_4Nb_2O_{13}$: a new ternary Se^{4+}–Nb^{5+}–oxide with monoselenite and diselenite groups. *Chemistry of Materials*, 1998, **10(2):** 646–649.
[21] BU KE-JUN, HUANG JIAN, LUO MENG-JIA, *et al*. Observation of high Seebeck coefficient and low thermal conductivity in [SrO]-intercalated $CuSbSe_2$ compound. *Chemistry of Materials*, 2018, **30(16):** 5539–5543.
[22] WANG QIN-CHAO, MENG JING-KE, YUE XIN-YANG, *et al*. Tuning P2-structured cathode material by Na-site Mg substitution for Na-Ion batteries. *Journal of the American Chemical Society*, 2019, **141(2):** 840–848.
[23] NAIK I, RASTOGI A K. Transport properties of 2H-$NbSe_2$: effect of Ga-intercalation. *Physica B: Condensed Matter*, 2010, **405(3):** 955–957.
[24] HAUDER J J, ROBBINS M, DISALVO F J. Effect of 3d impurities on the superconducting transition temperature of the layered compound $NbSe_2$. *Physical Review B*, 1973, **8(3):** 1038–1042.

Pd 插层 $NbSe_2$ 化合物的制备、晶体结构和电学性质研究

黄 冲[1,2], 赵 伟[1], 王 东[1], 卜克军[1,2], 王思顺[1], 黄富强[1,3]

(1. 中国科学院 上海硅酸盐研究所, 高性能陶瓷和超微结构国家重点实验室, 上海 200050; 2. 中国科学院大学, 北京 100049; 3. 北京大学 化学与分子工程学院, 北京分子科学国家实验室, 稀土材料化学及应用国家重点实验室, 北京 100871)

摘 要: 通过固相反应法合成一系列插层化合物 Pd_xNbSe_2 (x=0~0.17)。它们与 2H-$NbSe_2$ 相同, 属于六方晶格, 空间群为 $P6_3/mmc$。Pd 占据 $NbSe_2$ 层间的八面体空位。随着 Pd 含量的增加, 晶格常数 c 线性增大, 而 a 几乎不变。X 射线单晶衍射结果表明, $Pd_{0.17}NbSe_2$ 的晶格常数为 a=b=0.34611(2) nm, c=1.27004(11) nm。每个 Pd 原子与六个 Se 原子键合形成[$PdSe_6$]八面体来连接相邻的 Nb-Se 层, 使晶体结构变得更加稳定, 从而提高化合物的热稳定性。电学测试表明, 随着 Pd 含量的增加, Pd_xNbSe_2 的剩余电阻比减小。此外, 超导转变温度也随着 Pd 含量的增加而下降, 说明 Pd 的引入不利于 $NbSe_2$ 的超导态。

关 键 词: Pd_xNbSe_2; 过渡金属硫族化合物; 晶体结构; 超导

中图分类号: O782 **文献标识码:** A

Supporting information:

Synthesis, Crystal Structure, and Electrical Conductivity of Pd-intercalated $NbSe_2$

HUANG Chong[1,2], ZHAO Wei[1], WANG Dong[1], BU Ke-Jun[1,2], WANG Si-Shun[1], HUANG Fu-Qiang[1,3]

(1. State Key Laboratory of High Performance Ceramics and Superfine Microstructure, Shanghai Institute of Ceramics, Chinese Academy of Sciences, Shanghai 200050, China; 2. University of Chinese Academy of Sciences, Beijing 100049, China; 3. State Key Laboratory of Rare Earth Materials Chemistry and Applications, Beijing National Laboratory for Molecular Sciences, College of Chemistry and Molecular Engineering, Peking University, Beijing 100871, China)

Table S1　Fractional atomic coordinates and isotropic or equivalent isotropic displacement parameters of $Pd_{0.17}NbSe_2$

Atom	Wyck. Site	*x*	*y*	*z*	U_{iso}* or U_{eq}/nm^2	*Occ.*
Nb	*2b*	0	1	1/4	0.000075(2)	1
Se	*4f*	1/3	2/3	0.38104(5)	0.0000736(17)	1
Pd	*2a*	0	1	1/2	0.000059(11)	0.171(3)

Table S2　Atomic displacement parameters of $Pd_{0.17}NbSe_2$

	U_{11}/nm^2	U_{22}/nm^2	U_{33}/nm^2	U_{12}/nm^2	U_{13}/nm^2	U_{23}
Nb	0.000074(3)	0.000074(3)	0.000075(4)	0.0000372(13)	0	0
S	0.000064(2)	0.000064(2)	0.000094(3)	0.0000318(10)	0	0
Pd	0.000062(13)	0.000062(13)	0.000052(19)	0.000031(7)	0	0

Table S3　Geometric parameters for $Pd_{0.17}NbSe_2$

Bond	Distance/nm	Bond	Distance/nm
Nb1—Se2^{i}	0.26006(4)	Se2—Pd3^{viii}	0.25051(4)
Nb1—Se2^{ii}	0.26006(4)	Se2—Nb1^{viii}	0.26006(4)
Nb1—Se2^{iii}	0.26006(4)	Se2—Nb1^{vii}	0.26006(4)
Nb1—Se2^{iv}	0.26006(4)	Pd3—Se2^{ix}	0.25051(4)
Nb1—Se2	0.26006(4)	Pd3—Se2^{iv}	0.25051(4)
Nb1—Se2^{v}	0.26006(4)	Pd3—Se2^{x}	0.25051(4)
Nb1—Pd3^{vi}	0.31751(3)	Pd3—Se2^{i}	0.25051(4)
Nb1—Pd3	0.31751(3)	Pd3—Se2^{xi}	0.25051(4)
Se2—Pd3^{vii}	0.25051(4)	Pd3—Nb1^{xi}	0.31751(3)
Se2—Pd3	0.25051(4)		
Bond	**Angle/(°)**	**Bond**	**Angle/(°)**
Se2^{i}—Nb1—Se2^{ii}	134.813 (8)	Pd3^{viii}—Se2—Nb1	133.822 (3)
Se2^{i}—Nb1—Se2^{iii}	79.58 (2)	Nb1^{viii}—Se2—Nb1	83.434 (16)
Se2^{ii}—Nb1—Se2^{iii}	83.434 (16)	Pd3^{vii}—Se2—Nb1^{vii}	76.881 (6)
Se2^{i}—Nb1—Se2^{iv}	83.434 (16)	Pd3—Se2—Nb1^{vii}	133.822 (3)
Se2^{ii}—Nb1—Se2^{iv}	79.58 (2)	Pd3^{viii}—Se2—Nb1^{vii}	133.822 (3)
Se2^{iii}—Nb1—Se2^{iv}	134.813 (7)	Nb1^{viii}—Se2—Nb1^{vii}	83.434 (16)
Se2^{i}—Nb1—Se2	83.433 (16)	Nb1—Se2—Nb1^{vii}	83.434 (16)
Se2^{ii}—Nb1—Se2	134.812 (7)	Se2—Pd3—Se2^{ix}	92.612 (17)
Se2^{iii}—Nb1—Se2	134.812 (8)	Se2—Pd3—Se2^{iv}	87.388 (17)
Se2^{iv}—Nb1—Se2	83.433 (16)	Se2^{ix}—Pd3—Se2^{iv}	180.0
Se2^{i}—Nb1—Se2^{v}	134.812 (8)	Se2—Pd3—Se2^{x}	92.612 (17)
Se2^{ii}—Nb1—Se2^{v}	83.434 (16)	Se2^{ix}—Pd3—Se2^{x}	87.388 (17)
Se2^{iii}—Nb1—Se2^{v}	83.434 (16)	Se2^{iv}—Pd3—Se2^{x}	92.612 (17)

Bond	Angle/(°)	Bond	Angle/(°)
Se2^{iv}—Nb1—Se2^{v}	134.812 (8)	Se2—Pd3—Se2^{i}	87.388 (17)
Se2—Nb1—Se2^{v}	79.58 (2)	Se2^{ix}—Pd3—Se2^{i}	92.612 (17)
Se2^{i}—Nb1—Pd3^{vi}	129.790 (11)	Se2^{iv}—Pd3—Se2^{i}	87.388 (17)
Se2^{ii}—Nb1—Pd3^{vi}	50.210 (11)	Se2^{x}—Pd3—Se2^{i}	180.0
Se2^{iii}—Nb1—Pd3^{vi}	50.210 (11)	Se2—Pd3—Se2^{xi}	180.0
Se2^{iv}—Nb1—Pd3^{vi}	129.790 (11)	Se2^{ix}—Pd3—Se2^{xi}	87.388 (17)
Se2—Nb1—Pd3^{vi}	129.790 (11)	Se2^{iv}—Pd3—Se2^{xi}	92.612 (17)
Se2^{v}—Nb1—Pd3^{vi}	50.210 (11)	Se2^{x}—Pd3—Se2^{xi}	87.388 (17)
Se2^{i}—Nb1—Pd3	50.210 (11)	Se2^{i}—Pd3—Se2^{xi}	92.612 (17)
Se2^{ii}—Nb1—Pd3	129.790 (11)	Se2—Pd3—Nb1	52.909 (12)
Se2^{iii}—Nb1—Pd3	129.790 (11)	Se2^{ix}—Pd3—Nb1	127.092 (12)
Se2^{iv}—Nb1—Pd3	50.210 (11)	Se2^{iv}—Pd3—Nb1	52.908 (12)
Se2—Nb1—Pd3	50.210 (11)	Se2^{x}—Pd3—Nb1	127.092 (12)
Se2^{v}—Nb1—Pd3	129.790 (11)	Se2^{i}—Pd3—Nb1	52.908 (12)
Pd3^{vi}—Nb1—Pd3	180.0	Se2^{xi}—Pd3—Nb1	127.091 (12)
Pd3^{vii}—Se2—Pd3	87.388 (17)	Se2—Pd3—Nb1^{xi}	127.091 (12)
Pd3^{vii}—Se2—Pd3^{viii}	87.388 (17)	Se2^{ix}—Pd3—Nb1^{xi}	52.908 (12)
Pd3—Se2—Pd3^{viii}	87.388 (17)	Se2^{iv}—Pd3—Nb1^{xi}	127.092 (12)
Pd3^{vii}—Se2—Nb1^{viii}	133.822 (2)	Se2^{x}—Pd3—Nb1^{xi}	52.908 (12)
Pd3—Se2—Nb1^{viii}	133.822 (3)	Se2^{i}—Pd3—Nb1^{xi}	127.092 (12)
Pd3^{viii}—Se2—Nb1^{viii}	76.881 (6)	Se2^{xi}—Pd3—Nb1^{xi}	52.909 (12)
Pd3^{vii}—Se2—Nb1	133.822 (2)	Nb1—Pd3—Nb1^{xi}	180.0
Pd3—Se2—Nb1	76.881 (6)		

Symmetry codes: (i) x, y+1, z; (ii) x−1, y, −z+1/2; (iii) x, y+1, −z+1/2; (iv) x−1, y, z; (v) x, y, −z+1/2; (vi) −x, −y+2, z−1/2; (vii) x+1, y, z; (viii) x, y−1, z; (ix) −x+1, −y+2, −z+1; (x) −x, −y+1, −z+1; (xi) −x, −y+2, −z+1.

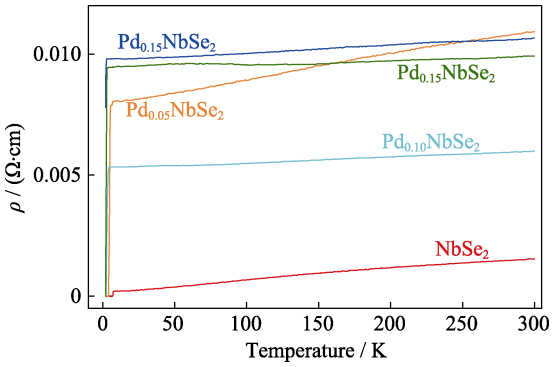

Fig. S1 Temperature dependence of the resistivity for Pd_xNbSe_2 ($0 \leqslant x \leqslant 0.17$)